Journal of Magnetic Resonance 308 (2019) 106593

Contents lists available at ScienceDirect

Journal of Magnetic Resonance

journal homepage: www.elsevier.com/locate/jmr

Rapid-scan EPR imaging of a phantom comprised of species with different linewidths and relaxation times

Yilin Shi, Sandra S. Eaton, Gareth R. Eaton *

Department of Chemistry and Biochemistry, University of Denver, Denver, CO 80210, USA

ARTICLE INFO

Article history:
Received 30 July 2019
Revised 5 September 2019
Accepted 6 September 2019
Available online 7 September 2019

Keywords:
Lithium phthalocyanine
Nitroxide
Triarylmethyl radical
Resonator bandwidth
Signal bandwidth

ABSTRACT

As a demonstration of the application of rapid-scan EPR to imaging at low frequency and magnetic field, a multi-compartment phantom containing six different samples was imaged. The samples were nitroxide radicals, trityl (substituted triarylmethyl) radicals, and the oxygen-sensitive solid lithium phthalocyanine (LiPc), all of which are useful for *in vivo* imaging. The 2D spectral-spatial image demonstration was performed at 250 MHz, with samples in sealed tubes of various sizes arranged in a 3D-printed plastic holder. Maximum gradients of 10 G/cm gave a spatial resolution of about 0.1 mm for the narrow trityl and LiPc signals and about 1 mm for the nitroxide. The importance of proper selection of resonator bandwidth and scan rate for obtaining accurate linewidth information is demonstrated for a case in which the phantom is composed of species with signal linewidths and relaxation times that differ by more than a factor of 10.

1. Introduction

Many physiologic parameters, such as O_2 concentration, pH, and tissue redox status have been monitored by imaging of nitroxide radicals, trityl (substituted triarylmethyl) radicals, LiPc (lithium phthalocyanine) and related O_2-responsive solids [1–4] and new probes are under development. Future experiments may develop bio-orthogonal labeling methods to measure multiple properties of cellular environments including O_2, pH, and redox status. It is important to determine how many of these parameters could be measured simultaneously or serially with spectroscopically distinguishable probes. Most oximetric imaging using trityl radicals has been performed using pulsed EPR [5]. Imaging of nitroxide radicals and LiPc and its analogs has been performed using continuous wave (CW) EPR until recently [1]. Prior work in this lab and in the Halpern lab has demonstrated the utility of rapid-scan EPR for imaging nitroxide radicals [6–8]. The NCI group has demonstrated direct-detected EPR with rotating gradients with 0.33 kHz sinusoidal scans [9]. In the present study we image a composite phantom containing all three types of radicals that have been used for in vivo imaging. From prior work it is known that trityls have longer relaxation times than nitroxides or LiPc. Approximate values for deoxygenated samples at about 20 °C at 250 MHz are T_1 = 12 μs and T_2 = 11.5 μs for trityl-CD_3 in aqueous solution [10], T_1 = 3.5 μs and T_2 = 2.5 μs for solid LiPc [11], and $T_1 \sim T_2 \sim 0.5$ μs for nitroxides in aqueous solution [12]. Linewidths for trityls and LiPc are about an order or magnitude smaller than for nitroxides. Thus, the rapid-scan response will be significantly different for these three types of samples.

2. Methods

The previously described home-built 250 MHz spectrometer [13–15], rapid-scan cross-loop resonator (CLR) for 25 mm diameter samples [16], and rapid-scan driver systems [17] were used. The resonator has a saddle coil for the excitation resonator and a fine wire, loop gap resonator for the receiver (detection) resonator. There is good separation of E (electric) and B (magnetic) fields and high isolation between the two resonators, permitting a wide range of sample types to be measured [16]. Resonator Q, measured with a HP network analyzer (HP 8719D), was 53 ± 1 for the excitation resonator, and 69 ± 2 for the signal detection resonator.

The sample holder (Fig. 1) was created using a 3D printer. The samples were in sealed tubes so the role of the holder was to support the tubes and it did not need to be liquid impermeable. For solvent impermeable applications we have found that HIPS (high impact polystyrene) is preferable to PLA (polylactic acid). The sample holder was designed using Sketchup software (Trimble Inc., https://www.sketchup.com). It was purposefully created with six compartments of three different sizes to hold samples of different sizes and shapes. The sample holder has an o.d. of 25 mm and is 75 mm long.

* Corresponding author at: Department of Chemistry and Biochemistry, University of Denver, 2101 E. Wesley Ave., Denver, CO 80210, USA.
E-mail address: geaton@du.edu (G.R. Eaton).

https://doi.org/10.1016/j.jmr.2019.106593
1090-7807/

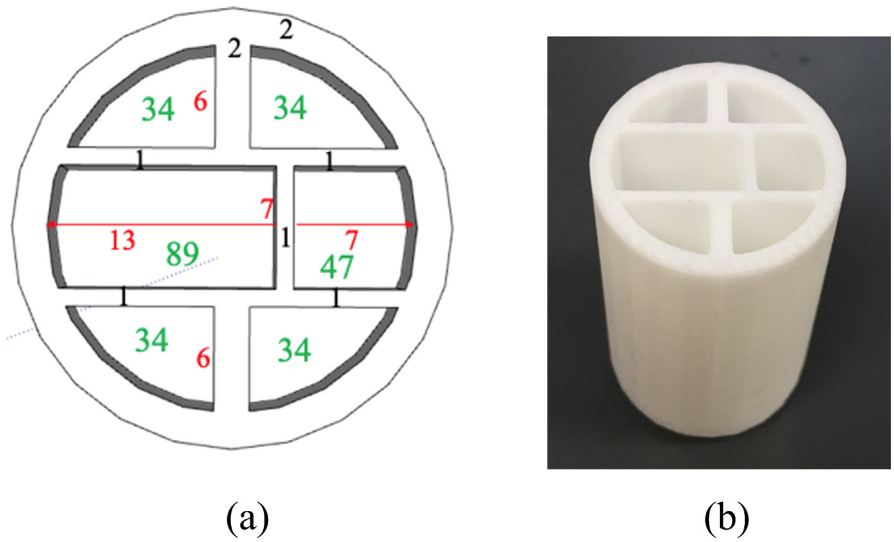

Fig. 1. Sample holder for 25 mm CLR. (a) Cross section of the sample holder. The red numbers (mm) are dimensions of the compartments; the black numbers (mm) are the divider or wall thickness; the green numbers are the cross-section area (mm^2) of each compartment, calculated from the Sketchup model. (b) Photograph of 3D printed sample holder constructed with HIPS. (For interpretation of the references to colour in this figure legend, the reader is referred to the web version of this article.)

The samples are listed in Table 1 and the structures are shown below.

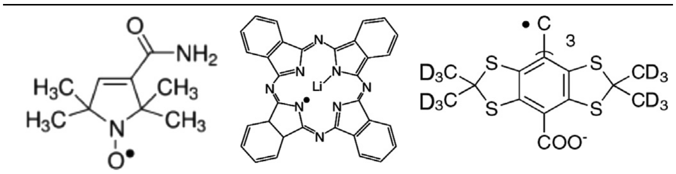

CTPO[a] LiPc Trityl-CD_3

[a]In mHCTPO the CH_3 groups are replaced by CD_3.

2.1. Parameter selection

With the sample holder and samples in the resonator, the resonant frequency was 262 MHz, so the magnetic center field for the image that encompassed all signals was 94 G. To include all three lines of the natural abundance nitroxide spectra, a 50 G rapid scan was used. Sinusoidal scans were selected because this permits wider scans for the same power to the scan coils [17] than for triangular scans. Scan frequencies in the range of 2.2–2.5 kHz were selected because these are in a range with relatively quiet mechanical resonator background [16] and a scan width of 50 G can be achieved at these frequencies. The inductance of the coils, L, was about 3.43 mH, but varied slightly with temperature. The resonance frequency of the coils was adjusted for each experiment. For example, a capacitance of 1.5 μF resonated the coils at 2.2 kHz as calculated using Eq. (1).

$$f = \frac{1}{2\pi\sqrt{LC}} \tag{1}$$

The resonator bandwidth is related to the Q by Eq. (2):

$$BW_{res} = \frac{v}{2Q} \tag{2}$$

where v is the RF frequency, Q is the quality factor of the resonator with sample. The factor of 2 is required because half of the bandwidth is used for the up-field scans and the other half is used for the down-field scans [18,19]. For the 25 mm rapid-scan cross loop sample resonator with Q = 69, BW_{res} = 1.9 MHz.

To avoid broadening the EPR spectrum in a rapid-scan experiment, it is necessary to choose data acquisition parameters such that the signal bandwidth is less than the resonator bandwidth [19,20]. The maximum scan rate (Eq. (3)) of a 50 G sinusoidal scan at 2.2 kHz is:

$$scan\ \ rate = \pi \times w \times f = 0.35\ \ \mathrm{MG/s} \tag{3}$$

where w is the scan width in gauss, f is the rapid-scan frequency. Signal bandwidth is calculated as:

$$BW_{sig} = \frac{N \times scan\ \ rate}{\pi \times LW} \tag{4}$$

where LW is the full linewidth at half height (FWHH) of the rapid-scan absorption signal. The FWHH linewidths (Table 1) were

Table 1
Properties of samples in the imaging phantom.

#	Sample[a]	Scan width (G)	FWHH[b] (mG)	BW_{sig}[c] (MHz)
(a)	0.53 mM CTPO in H_2O, 5 mm OD	50	1300	0.42
(b)	0.2 mM CTPO in H_2O, 5 mm OD	50	1200	0.46
(c)	0.2 mM ^{15}N CTPO-d_{13} in ethanol, 4 mm OD	50	400	1.38
(d)	0.2 mM trityl-CD_3 in H_2O, 4 mm OD	5	40	1.38
(e)	0.5 mM ^{15}N mHCTPO-d_{12} in H_2O, 5 mm OD	50	900	0.61
(f)	particles of LiPc, 4 mm OD tube	5	70	0.79

[a] OD is the outside diameter of the tube that contains the sample.
[b] The full-width at half height (FWHH) linewidth was measured in 2.2 kHz scans.
[c] Signal bandwidth for scan width listed.

obtained from scans of the individual tubes that comprised the phantom at rates that were slow enough to provide unbroadened lines. The larger the factor *N*, the more conservative the result. We commonly set N to 5, which was the value used for the calculations discussed here. The narrower the signal, and the higher the scan rate, the higher the signal bandwidth. The signal bandwidths for the samples in the phantom are summarized in Table 1.

Based on power saturation curves the incident RF power was selected (0.103 mW which is 2.54 mG B_1) such that all signals were in the linear response regime. This low power was limited by the long relaxation times of the trityl sample. Spectra were digitized in a Bruker SpecJet-II digitizer. A 20 ns time base and 65,536 points were used so that at about 2.2 kHz, one scan contains 3 full sinusoidal cycles, which is preferred for the deconvolution software [18,21]. The gradient coils and CAEN power supply (FAST-PS-2040-600) provided a maximum gradient of 10 G/cm. Projections were acquired at equally spaced increments in gradient and constant magnetic field scan width. The projections were deconvolved as described in [21]. The 2D spectral-spatial images were reconstructed as previously reported [22] and displayed without amplitude thresholding. The images are constructed on grids with 4000 points along the spectral axis and 180 points along the spatial axis.

3. Results

To characterize the spectral components in the absence of gradient the linewidth of the signals from each sample was measured individually using a slow scan frequency and appropriate scan width (Table 1). These scans satisfied the criterion that the signal bandwidths were less than the resonator bandwidth. The natural abundance CTPO samples exhibit a 3-line spectrum due to splitting by the ^{14}N with I = 1. Due to Breit-Rabi effects [23], the three lines have an asymmetric splitting pattern at 250 MHz. The splittings between low-field and center-field, and center-field to high-field lines were 14.8 and 17.6 G, respectively, for a total spacing of 32.4 G [24]. The CTPO samples have linewidths of about 1200 mG due to unresolved proton hyperfine couplings, which is consistent with literature reports [12]. The linewidth is slightly narrower for the 0.2 mM sample than for 0.53 mM. The ^{15}N CTPO-d_{13} has a 2-line spectrum due to splitting by the ^{15}N with I = 0.5 and the spacing between the two lines is 22.6 G [24]. The linewidth is narrower for ^{15}N CTPO-d_{13} than for CTPO because of the deuteration of the methyl groups. The apparent linewidth for ^{15}N mHCTPO-d_{12} is larger than for ^{15}N CTPO-d_{13} because of partially resolved splitting by the 4-H on the ring [25]. The trityl-CD_3 line has FWHH of 40 mG which is good agreement with the reported value of FWHH = 34 mG and ΔB_{pp} = 24 mG [11]. The signal from the multiparticle LiPc sample has FWHH of 70 mG. This value is somewhat larger than the previously reported values at 250 MHz of FWHH = 44 mG and ΔB_{pp} 34 = mG [11]. The sample of LiPc that was used in the current experiments was from a different batch than the literature report. Linewidths for LiPc are very sensitive to preparation and vary from batch to batch.

The signal bandwidth should be less than resonator bandwidth to avoid line broadening. The signal bandwidths summarized in Table 1 show that a 50 G scan at about 2.2 kHz will not broaden the lines for the nitroxides. However, for the trityl and LiPc samples, the spectra are broadened by the 50 G scan width that was selected for imaging the full nitroxide spectra. The effect of scan width on linewidth at constant scan frequency was demonstrated by comparing the deconvolved line widths for Trityl and LiPc at three selected scan widths (Table 2).

The selection of imaging parameters is an example of the need to optimize acquisition conditions for the desired information about the sample. If the primary interest is the nitroxide linewidth, and one needs merely the spatial location, not the precise linewidth, of the narrow trityl or LiPc sample, then the wider scan is appropriate. If the width of the trityl or LiPc signal is also needed to measure $[O_2]$ concentration, for example, then it is also necessary to scan the central region of the spectrum more slowly, by changing either the scan width or the scan frequency. Once the coils are resonated with the capacitors, changing the scan width is easier. The impact of scan width on linewidth is illustrated in the following two images.

3.1. 2D spectral-spatial image with 50 G scan width

A 6-sample phantom was assembled with the geometry shown in Fig. 2. Since this is a proof-of-principle application of rapid-scan EPR to the diverse sample types, only a 2D spectral-spatial image was obtained. The magnetic field axis is defined as the *Z* direction and a gradient along the *Z* axis was used to acquire the projections for a 2D spectral-spatial image (Fig. 2) in which the signals from all six samples are resolved. The shadow of the image along the spectral axis is in good agreement with the spectrum for the phantom in the absence of gradient. In the spectral shadow the signals from the two tubes containing CTPO are fully overlapped. The nitrogen hyperfine splitting is slightly larger for ^{15}N mHCTPO-d_{12} in water than for ^{15}N CTPO-d_{13} in ethanol so the doublet splitting for mHCTPO is partially resolved from the single line for CTPO. The very sharp lines for trityl-CD_3 and LiPc are fully overlapped. The positions of the three pairs of tubes in the phantom are well resolved in the spatial shadow. Spatial slices at the magnetic fields that correspond to the low-field ^{15}N nitroxide line, the overlapping trityl and LiPc lines and the high-field line for ^{14}N-CTPO accurately reflect the *Z*-axis positions of the tubes containing the respective samples.

The linewidths of each sample in the spectral slices through the image in Fig. 2 are summarized in Table 3. For the nitroxides, the linewidths are in reasonable agreement with the values observed for the samples individually, which confirms that the imaging procedure accurately captured the spectral information. However, for the trityl and LiPc samples the linewidths were broadened as predicted by the calculations that showed signal bandwidths greater than resonator bandwidth at these relatively rapid scan rates. In addition, the use of 65,535 points/3 cycles for 50 G scans corresponds to about 13 mG/point which limits the accuracy with which narrow lines can be reconstructed in the image. The spatial lengths of the features in the image that corresponding to samples a, b, e (in 5 mm OD tubes) were 4.0 mm, for features c and d (in 4 mm

Table 2
Impact of scan width at 2.4 kHz on apparent FWHH of narrow signals.

Scan width (G)	BW_{res} (MHz)	Trityl-CD_3		LiPc	
		BW_{sig} (MHz)	Observed FWHH (mG)	BW_{sig} (MHz)	Observed FWHH (mG)
5	1.9	1.5	40	0.86	70
20	1.9	6	82	2.89	108
50	1.9	15	187	7.2	220

Parameters: rapid-scan frequency is 2.4 kHz, time base 20 ns, 65,536 points for three full cycles, 4096 averages.

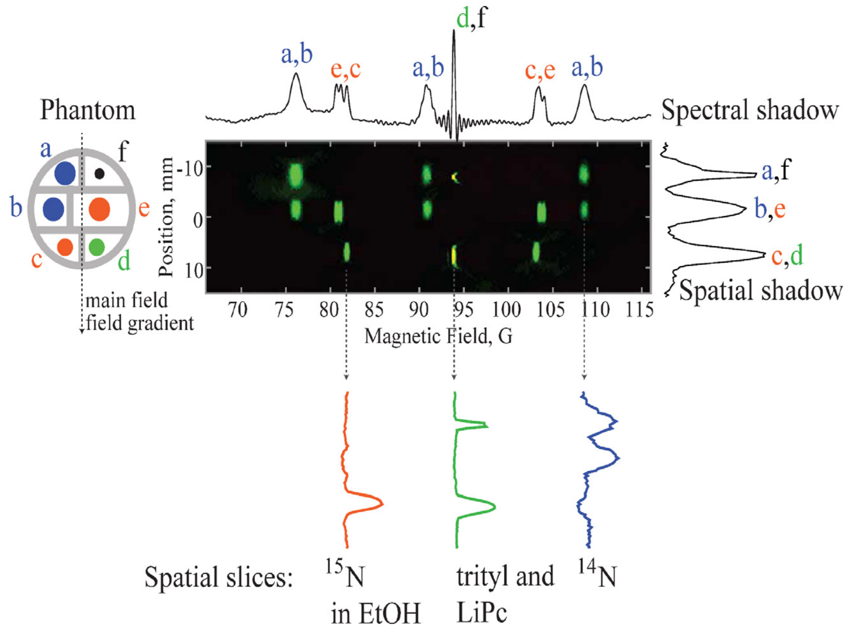

Fig. 2. Sample arrangement in phantom and 2D spectral-spatial image showing all six samples. The arrow marks the direction of B_o and of the magnetic field gradient. Parameters: 50 G scan width, 2.2 kHz rapid-scan frequency, time base 20 ns, 65,536 points for three full cycles, 8192 averages for each projection; Gmax = 10 G/cm with 0.05 G/cm step, 401 total projections.

Table 3
Linewidth of signals in spectral slices from image with 50 G spectral window (Fig. 2).

#	Sample	FWHH (mG)
(a)	0.53 mM CTPO in H_2O	1250
(b)	0.2 mM CTPO in H_2O	1200
(c)	0.2 mM ^{15}N CTPO in ethanol	530
(d)	0.2 mM trityl-CD_3 in H_2O	340[a]
(e)	0.5 mM ^{15}N mHCTPO in H_2O	960
(f)	particles of LiPc	320[a]

[a] In 50 G scans at 2.2 kHz the signal bandwidth is greater than resonator bandwidth for trityl-CD_3 and LiPc, which broadens these signals.

OD tubes) were 3.3 mm, and for polycrystalline sample f (in 1 mm ID capillary) was 1 mm. The spatial dimensions are in good agreement with the dimensions of the tubes, which have wall thickness of about 0.38–0.5 mm.

3.2. 2D spectral-spatial image with 5 G scan width

To avoid line broadening for the sharpest lines, we need a slower scan rate, which can be achieved by acquiring projections with a narrower scan width. Alternatively a lower scan frequency could have been used, but that would not benefit from the advantages of rapid scans. EPR imaging with a 5 G scan width and 2.2 kHz scan frequency was performed to capture only the trityl and LiPc signals (Fig. 3). Although the middle line of the ^{14}nitroxide spectrum is partially included in these 5 G scans, it is so broad relative to the signals from trityl and LiPc that it was deleted by the background correction routine. At a Zeeman frequency of 262 MHz both trityl and LiPc have a resonant field of about 94 G, but the two tubes are well separated along the spatial dimension. The peak at about Z = 7.2 mm comes from trityl and the peak at about −9.1 mm is LiPc. From the spectral slices, the FWHH linewidths are 67 mG for LiPc and 69 mG for trityl-CD_3, which are substantially narrower than in the image with the 50 G spectral window (Table 3). However, the linewidth for the trityl sample is significantly broader than for the individual sample in spectra about with 5 G scans, which is attributed to the limited number of projections. The linewidth for the LiPc sample is close to what was observed for the individual sample in a 5 G wide scan.

The spatial length in the image for the trityl sample is 3.3 mm, which is consistent with the expected ID of the 4 mm OD tube. For the LiPc sample the spatial length is about 1 mm, which is

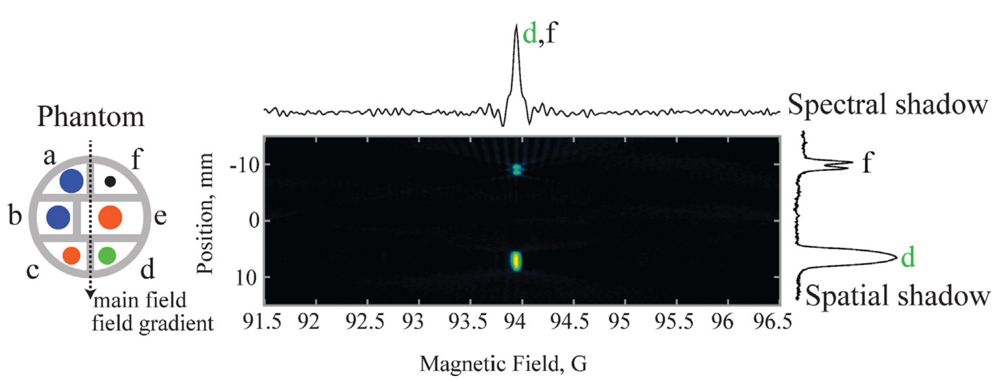

Fig. 3. EPR image with 5 G spectral window. The arrow marks the direction of B_o and of the magnetic field gradient. Parameters: 94 G center field, 5G scan width, Gmax = 10 G/cm with 0.05 G/cm step, 401 projections, 8192 averages for each projection, 20 ns time base and 65,536 points for three cycles.

Table 4
Linewidths in spectral slice of image with different numbers of projections.

Number of Projections	Gradient step (G/cm)	Observed FWHH (mG)		Total data acquisition time (min)
		Trityl-CD_3	LiPc	
201	0.1	93	83	93
401	0.05	69	67	186
2001	0.01	55	67	878

Parameters: 5 G scan width, 2.45 kHz scan frequency; 20 ns time base, 65,536 points for three cycles and 8192 averages; gradient strength Gmax = 10 G/cm. The number of pixels along spectral axis is 4000, which is 800 pts/gauss.

consistent with the accidental distribution of two clumps of LiPc particles. The blurring of the spatial distribution is due to the distribution of particles. The particles tend to cling to the walls of the capillary which results in higher probability near the walls of the capillary than in the center. The features in the image are separated by about 16.5 mm, which is in good agreement with the positions of the tubes containing the LiPc and trityl samples. For the peak corresponding to trityl on the spatial shadow, the bottom of the peak is 5.3 mm wide, the width at half height is 3.3 mm. The broadening at the base may reflect contributions from imperfections in the image.

The resolution of the image can be estimated from the ratio of the maximum gradient (10 G/cm) to the linewidths of the signals. For the trityl and LiPc samples the linewidths are about 0.1 G so the calculated resolution is about 0.1 mm. For the nitroxide samples the linewidths are about 1 G so the calculated resolution is about 1 mm. For both types of samples the much resolution is better than the separations between samples.

3.3. Impact of increasing the number of projections

For the spectral slice of an image, increasing the number of projections (Table 4) narrows the linewidth for signals with very sharp lines. For our current CAEN power supplies and the minimum resolution for stepping the current, the gradient resolution is limited to 0.01 G/cm. For a maximum gradient of 10 G/cm the maximum number of steps in the gradient produces 2001 projections. The impact on the linewidths of changing the number of projections is shown in Table 4. For the LiPc signal there is no advantage of increasing the number of projections beyond 401, but there is a small improvement in linewidth accuracy for the trityl-CD_3 of further increasing the number of projections.

Increasing the number of projections, also increases the data acquisition times. For the total data acquisition time listed in Table 4, 53% of the time is used by the digitizer to acquire data, and 47% of the time is used for exporting data from the digitizer to the computer. For each projection it takes 14.52 s to acquire data, while the theoretical time = 20 ns $\times$ 65536 points $\times$ 8192 averages = 10.74 s, so the digitizer efficiency is 10.74/14.52 = 74%. The overhead is due to the way the digitizer is designed and built. A digitizer with more efficient data transfer rates could decrease the experimental overhead.

Because the samples are all in sealed thin tubes, the gap between the tubes are large enough to allow them to be completely separated from each other on the spatial axis of the image, whatever number of projections were used.

4. Summary

2D spectral spatial imaging was performed for a phantom containing six samples with different hyperfine splitting, CW line shapes, relaxation times, concentrations, and sizes. The experiments demonstrate that the scan rates and numbers of projections need to be selected to be appropriate for the properties of the species imaged and the goal of the imaging experiment. The rapid-scan deconvolution method and the EPR imaging method, which was designed for multiline spectra at low field, produce reliable results for this range of relaxation times provided that the scan rates are chosen appropriately.

Rapid scan provides substantially improved signal-to-noise relative to continuous wave EPR for a wide range of samples [19,26,27]. Pulsed experiments provide comparable signal-to-noise per unit time for samples such as trityl with narrow-enough lines that they can be fully excited by RF/microwave pulses. However, for some pulse amplifiers, limitations of duty cycle attenuate the expected advantages of pulsed EPR. The trityls were used in the present measurements as convenient and well-characterized narrow-line samples and demonstrate compatibility with rapid scan. We judge that pulsed EPR is the method of choice for in vivo oximetry using currently available trityl radicals. Nitroxide relaxation times at frequencies appropriate for in vivo imaging are so short, that pulse experiments are challenging. For nitroxides rapid scan is likely to be the method of choice for in vivo imaging.

Acknowledgements

This research was supported by NIH NCI grant R01CA177744. The instrumentation was constructed by Dr. George A. Rinard and Richard W. Quine, as described in the literature cited. The sample holder was 3D printed by Dr. Rinard. The software used for image reconstruction was originally written by Dr. Mark Tseitlin. The LiPc was a gift from Prof. Harold Swartz, Dartmouth College.

References

[1] B. Epel, H.J. Halpern, In vivo pO2 imaging of tumors: oxymetry with very low frequency electron paramagnetic resonance, Meth. Enzymol. 254 (2016) 501–527.
[2] A.A. Bobko, T.D. Eubank, J.L. Voorhees, O.V. Efimova, I.A. Kirilyuk, S. Petryakov, D.G. Trofimiov, C.B. Marsh, J.L. Zweier, I.A. Grigorev, A. Samouilov, V.V. Khramtsov, In vivo monitoring of pH, redox status, and glutathione using L-band EPR for assessment of therapeutic effectiveness in solid tumors, Magn. Reson. Med. 67 (2012) 1827–1836.
[3] N. Khan, H. Hou, H.M. Swartz, P. Kuppusamy, Direct and repeated measurement of heart and brain oxygenation using in vivo EPR oximetry, Meth. Enzymol. 564 (2015) 529–552.
[4] B. Epel, H.J. Halpern, EPR imaging, in: D. Goldfarb, S. Stoll (Eds.), EPR Spectroscopy: Fundamentals and Methods, John Wiley & Sons, West Sussex, U.K., 2018, pp. 261–275.
[5] B. Epel, M.K. Bowman, C. Mailer, H.J. Halpern, Absolute oxygen R1e imaging *in vivo* with pulse electron paramagnetic resonance, Magn. Reson. Med. 72 (2014) 362–368.
[6] J.R. Biller, M. Tseitlin, R.W. Quine, G.A. Rinard, H.A. Weismiller, H. Elajaili, G.M. Rosen, J.P. Kao, S.S. Eaton, G.R. Eaton, Imaging of nitroxides at 250 MHz using rapid-scan electron paramagnetic resonance, J. Magn. Reson. 242 (2014) 162–168.
[7] H.B. Elajaili, J.R. Biller, G.M. Rosen, J.P.Y. Kao, M. Tseytlin, L.A. Buchanan, G.A. Rinard, R.W. Quine, J. McPeak, Y. Shi, S.S. Eaton, G.R. Eaton, Imaging disulfide dinitroxides at 250 MHz to monitor redox status, J. Magn. Reson. 260 (2015) 77–82.
[8] B. Epel, S.V. Sundramoorthy, M. Krzykowska-Serda, M.C. Maggio, M. Tseytlin, G.R. Eaton, S.S. Eaton, G.M. Rosen, J.P.Y. Kao, H.J. Halpern, Imaging thiol redox status in murine tumors in vivo with rapid-scan electron paramagnetic resonance, J. Magn. Reson. 276 (2017) 31–36.
[9] S. Subramanian, J. Koscielniak, N. Devasahayam, R.H. Pursley, T.J. Pohida, M. Krishna, A new strategy for fast CW EPR imaging: direct detection with

simultaneous rapid-scan and rotating gradients, J. Magn. Reson. 186 (2007) 212–219.
[10] R. Owenius, G.R. Eaton, S.S. Eaton, Frequency (250 MHz to 9.2 GHz) and viscosity dependence of electron spin relaxation of triarylmethyl radicals at room temperature, J. Magn. Reson. 172 (2005) 168–175.
[11] J.W. Stoner, D. Szymanski, S.S. Eaton, R.W. Quine, G.A. Rinard, G.R. Eaton, Direct-detected rapid-scan EPR at 250 MHz, J. Magn. Res. 170 (2004) 127–135.
[12] J.R. Biller, H. Elajaili, V. Meyer, G.M. Rosen, S.S. Eaton, G.R. Eaton, Electron spin lattice relaxation mechanisms of rapidly-tumbling nitroxide radicals, J. Magn. Reson. 236 (2013) 47–56.
[13] R.W. Quine, G.A. Rinard, S.S. Eaton, G.R. Eaton, A pulsed and continuous wave 250 MHz electron paramagnetic resonance spectrometer, Magn. Reson. Engineer 15 (2002) 59–91.
[14] G.A. Rinard, R.W. Quine, G.R. Eaton, S.S. Eaton, 250 MHz crossed loop resonator for pulsed electron paramagnetic resonance, Magn. Reson. Engineer 15 (2002) 37–46.
[15] R.W. Quine, G.A. Rinard, S.S. Eaton, G.R. Eaton, Quantitative rapid scan EPR spectroscopy at 258 MHz, J. Magn. Reson. 205 (2010) 23–27.
[16] L.A. Buchanan, L.B. Woodcock, G.A. Rinard, R.W. Quine, Y. Shi, S.S. Eaton, G.R. Eaton, 250 MHz rapid scan cross loop resonator, Appl. Magn. Reson. 50 (2019) 333–345.
[17] R.W. Quine, D.G. Mitchell, S.S. Eaton, G.R. Eaton, A resonated coil driver for rapid scan EPR, Conc. Magn. Reson., Magn. Reson. Engineer 41B (2012) 95–110.
[18] M. Tseitlin, D.G. Mitchell, S.S. Eaton, G.R. Eaton, Corrections for sinusoidal background and non-orthogonality of signal channels in sinusoidal rapid magnetic field scans, J. Magn. Reson. 223 (2012) 80–84.
[19] S.S. Eaton, R.W. Quine, M. Tseitlin, D.G. Mitchell, G.A. Rinard, G.R. Eaton, Rapid scan electron paramagnetic resonance, in: S.K. Misra (Ed.), Multifrequency Electron Paramagnetic Resonance: Data and Techniques, Wiley, 2014, pp. 3–67.
[20] G.R. Eaton, S.S. Eaton, Rapid scan electron paramagnetic resonance, eMagRes 5 (2016) 1529–1542.
[21] M. Tseitlin, G.A. Rinard, R.W. Quine, S.S. Eaton, G.R. Eaton, Deconvolution of sinusoidal rapid EPR scans, J. Magn. Reson. 208 (2011) 279–283.
[22] M. Tseitlin, J.R. Biller, H. Elajaili, V. Khramtsov, I. Dhimitruka, G.R. Eaton, S.S. Eaton, New spectral-spatial imaging algorithm for full EPR spectra of multiline nitroxides and pH sensitive trityl radicals, J. Magn. Reson. 245 (2014) 150–155.
[23] D. Gillies, L. Sutcliffe, M. Symms, Effects encountered in EPR spectroscopy and imaging at small magnetic fields, JCS Faraday Trans. 90 (1994) 2671–2675.
[24] M. Tseitlin, J.R. Biller, H. Elajaili, V.V. Khramtsov, I. Dhimitruka, G.R. Eaton, S.S. Eaton, New spectral–spatial imaging algorithm for full EPR spectra of multiline nitroxides and pH sensitive trityl radicals, J. Magn. Reson. 245 (2014) 150–155.
[25] Y.J. Lin, B.A. Teicher, H.J. Halpern, Synthesis of 4-protio-3-carbamoyl-2,2,5,5-tetraperdeuteromethyl-3-pyrrolin-1-yloxy (mHCTPO): a selectively isotopically labeled compound for use in T_2 spin label oxymetry, J. Labelled Compds Radiopharm. 28 (1990) 621–631.
[26] J.R. Biller, D.G. Mitchell, M. Tseytlin, H. Elajaili, G.A. Rinard, R.W. Quine, S.S. Eaton, G.R. Eaton, Rapid scan electron paramagnetic resonance opens new avenues for imaging physiologically important parameters in vivo, J. Visualized Exp. E54068 (2016), https://doi.org/10.3791/54068.
[27] D.G. Mitchell, M. Tseitlin, R.W. Quine, V. Meyer, M.E. Newton, A. Schnegg, B. George, S.S. Eaton, G.R. Eaton, X-band rapid-scan EPR of samples with long electron relaxation times: a comparison of continuous wave, pulse, and rapid-scan EPR, Mol. Phys. 111 (2013) 2664–2673.